

# $\mu$ -Analysis and Synthesis of a Flexible Beam Magnetic Suspension System

M. FUJITA, F. MATSUMURA AND T. NAMERIKAWA

## ABSTRACT

This paper is concerned with  $\mu$ -analysis and synthesis of a flexible beam magnetic suspension system. The experimental apparatus utilized in this study is a simplified model of magnetic bearings with an elastic rotor. After introducing the apparatus, a nominal model as well as a set of plant models which accounts for additive model uncertainty, is derived. We then setup robust performance objective as a structured singular value ( $\mu$ ) test. There, for all the possible plant models, the closed-loop system is required to be internally stable, and in addition, the weighted sensitivity is required to satisfy a certain  $H_\infty$ -norm condition. For the design, we make use of an iterative computing environment  $\mu$ -Analysis and Synthesis Toolbox, where the so-called  $D$ - $K$  iteration approach is employed. The designed controller is implemented using a digital signal processor  $\mu$ PD77230. Several experiments are carried out in order to evaluate robust performance of this design. These experimental results show that the closed-loop system achieves robust performance against various real perturbations.

## 1. INTRODUCTION

The progress of  $\mu$ -control theory, as well as the concepts of LFTs and LMIs [1], now produces a powerful computing environment  $\mu$ -Analysis and Synthesis Toolbox [2]. In this situation, the application of  $\mu$  to the magnetic suspension technology is one of the most challenging issues. In this paper, a  $\mu$ -controller is experimentally evaluated on a magnetic suspension system with a flexible beam. Based on several experimental results, we will show that the closed-loop system designed by  $\mu$ -synthesis achieves robust performance against various real perturbations.

## 2. FLEXIBLE BEAM MAGNETIC SUSPENSION SYSTEM

We consider a magnetic suspension system with a flexible beam shown in Figure 1 [3] - [5]. The experimental configuration consists of a flexible aluminum beam with an electromagnet and a gap sensor, which is a simplified model of magnetic bearings for a flexible rotor. The beam is supported by a hinge at the left side. Mass  $M$  is attached at the center of the beam and mass  $m$  is attached at the right side. An U-shaped electromagnet is located as an actuator at the right side. As a gap sensor, a standard induction probe of eddy-current type is placed at the same position in the right side. The nominal parameters are given in TABLE I.

---

Masayuki Fujita, Fumio Matsumura, and Toru Namerikawa, Department of Electrical and Computer Engineering, Kanazawa University, Kodatsuno 2-40-20, Kanazawa 920, Japan

TABLE I - NOMINAL PARAMETERS.

beam length $2l$ , m	3.8
first order resonance frequency $f_n$ , Hz	4.5
deflection of the beam $X_2$ , m	$12.3 \times 10^{-3}$
mass $m$ , kg	5.8
mass $M$ , kg	10.36
stationary gap of the electromagnet $X_1$ , m	$5.0 \times 10^{-3}$
steady state current of the electromagnet $I$ , A	0.885
resistance of the electromagnet $R$ , $\Omega$	57
inductance of the electromagnet $L$ , H	3.16

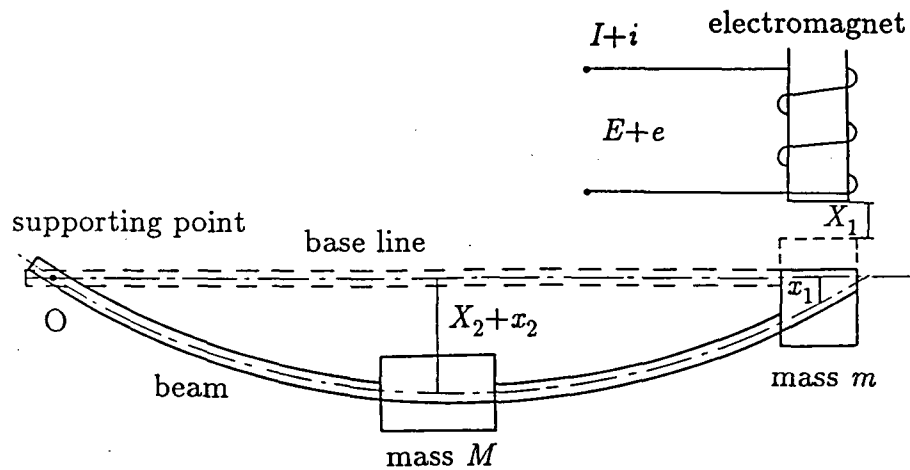


Figure 1. Flexible beam magnetic suspension system.

A digital signal processor (DSP)-based real-time controller is implemented with NEC  $\mu$ PD77230, which can execute one instruction in 150 ns with 32-bit floating point arithmetic. The data acquisition boards consist of a 12-bit A/D converter DATEL ADC-B500 with the maximum conversion speed of  $0.8 \mu$ s, and a 12-bit D/A converter DATEL DAC-HK12 with the maximum conversion speed of  $3 \mu$ s.

### 3. MODELS

#### 3.1. NOMINAL MODEL

A nominal model of this experimental system has been derived in [3], [4]. The state-space representation is of the following form

$$\dot{x}_g = A_g x_g + B_g u, \quad y = C_g x_g \quad (1)$$

where  $x_g := [x_1 \ x_2 \ \dot{x}_1 \ \dot{x}_2 \ i]^T$ ,  $u := e$ ,  $y := x_1$ , and

$$A_g = \begin{bmatrix} 0.0 & 0.0 & 1.0 & 0.0 & 0.0 \\ 0.0 & 0.0 & 0.0 & 1.0 & 0.0 \\ 7070 & 712 & -0.327 & 0.654 & -41.9 \\ 399 & -797 & 0.654 & -1.31 & 0.0 \\ 0.0 & 0.0 & 0.0 & 0.0 & -18.0 \end{bmatrix}, \quad B_g = \begin{bmatrix} 0.0 \\ 0.0 \\ 0.0 \\ 0.0 \\ 0.317 \end{bmatrix}, \quad C_g = [1 \ 0 \ 0 \ 0 \ 0]. \quad (2)$$

With this, the nominal transfer function  $G_{nom}$  from  $u$  to  $y$  can be obtained as follows

$$G_{nom} = \frac{-13.3(s+0.654-j28.2)(s+0.654+j28.2)}{(s+84.4)(s-84.1)(s+18.0)(s+0.697-j28.8)(s+0.697+j28.8)} \quad (3)$$

### 3.2. MODEL PERTURBATIONS

There is no need to say that discrepancies exist between the nominal model and the real plant depicted in Figure 1. These uncertainties may be due to the unmodeled dynamics of the flexible beam, and the neglected nonlinearities in the electromagnet. In order to account for these two types of inaccuracies, the following model perturbations have been employed.

Define the transfer function  $G_{m\_perturb}$  and  $G_{r\_perturb}$  from  $G_{nom}$  with two model parameters changed ( see TABLE I ). There, in the former the parameter  $m$  was replaced by  $1.5m$  (i.e., 50% increase), and in the latter the parameter  $R$  was replaced by  $1.05R$  (i.e., 5% increase). Using these perturbed transfer functions, define

$$\Delta_m := G_{m\_perturb} - G_{nom}, \quad \Delta_R := G_{r\_perturb} - G_{nom} \quad (4)$$

Each magnitude of these additive perturbations  $\Delta_m$  and  $\Delta_R$  are plotted in Figure 2.

### 3.3. SET OF PLANT MODELS

Now consider the set of plant models as

$$\mathbf{G} := \{ G_{nom} + \Delta_{add} W_{add} : \| \Delta_{add} \|_{\infty} \leq 1 \} \quad (5)$$

in which the real plant is assumed to reside ( see Figure 3 ). Here the transfer function  $\Delta_{add} W_{add}$  represents the potential differences between the nominal model  $G_{nom}$  and the actual behavior of the real plant. All of the uncertainty is captured in the normalized, unknown transfer function  $\Delta_{add}$ . From Figure 2, the uncertainty weighting  $W_{add}$  is chosen as follows

$$W_{add} = \frac{6.2 \times 10^{-6} (1+s/5.0)(1+s/550.0)(1+s/700.0)}{(1+s/30.0)(1+s/35.0)(1+s/38.0)} \quad (6)$$

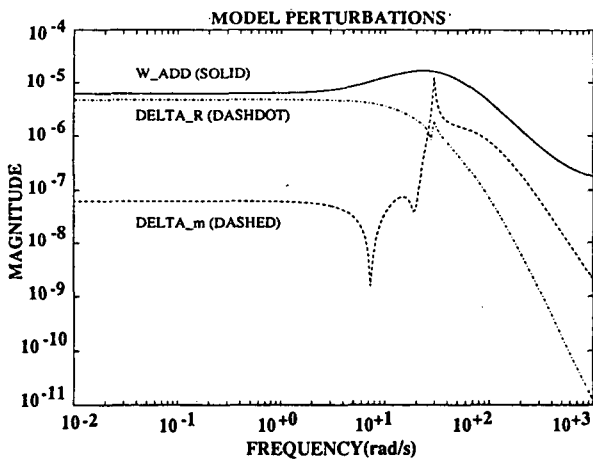


Figure 2. Model perturbations.

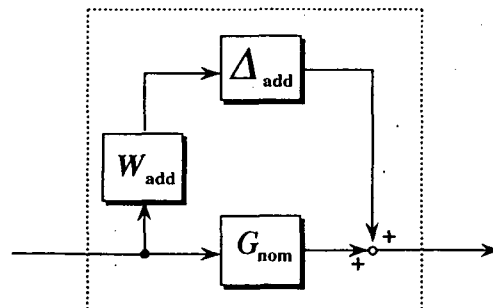


Figure 3. Set of plant models.

## 4. PROBLEM SETUP

### 4.1. DESIGN OBJECTIVES

Consider the feedback structure shown in Figure 4. The dashed box represents the transfer function of the real flexible beam magnetic suspension system, which is unstable in nature. Hence, our principal control objective is its stabilization. In fact, we would like to design a stabilizing controller  $K$  not only for the nominal model  $G_{nom}$ , but for all the possible plant models  $G \in \mathbf{G}$ . This robust stability condition is equivalent to

$$\| W_{add_r} K(I+G_{nom}K)^{-1} W_{add_l} \|_\infty < 1. \quad (7)$$

It is noted in Figure 4 that we factor the uncertainty weighting as  $W_{add} = W_{add_l} W_{add_r}$  where  $W_{add_l} = 1.0 \times 10^{-7}$ .

The performance of this feedback system can be evaluated using the (output) sensitivity function

$$S := (I+G_{nom}K)^{-1}. \quad (8)$$

In order to reject disturbances at low frequency, the performance weighting  $W_{perf}$  is chosen as

$$W_{perf} = \frac{20.0}{(1+s/0.1)}. \quad (9)$$

( see Figure 5 ). Factoring  $W_{perf} = W_{perf_l} W_{perf_r}$  with  $W_{perf_l} = 1.0 \times 10^{-7}$ , the nominal performance requirement is then equivalent to

$$\| W_{perf_r} (I+G_{nom}K)^{-1} W_{perf_l} \|_\infty < 1. \quad (10)$$

In practical situation, however, we would like to achieve this performance for all the possible plant models  $G \in \mathbf{G}$ :

$$\| W_{perf_r} (I+GK)^{-1} W_{perf_l} \|_\infty < 1, \quad \forall G \in \mathbf{G}. \quad (11)$$

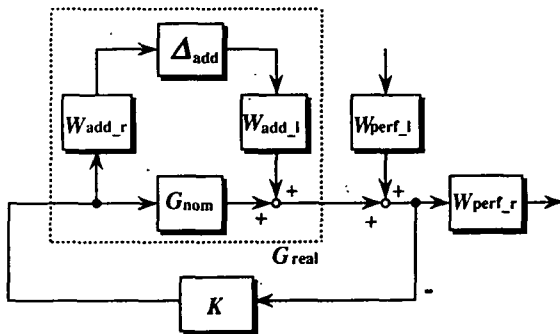


Figure 4. Feedback structure.

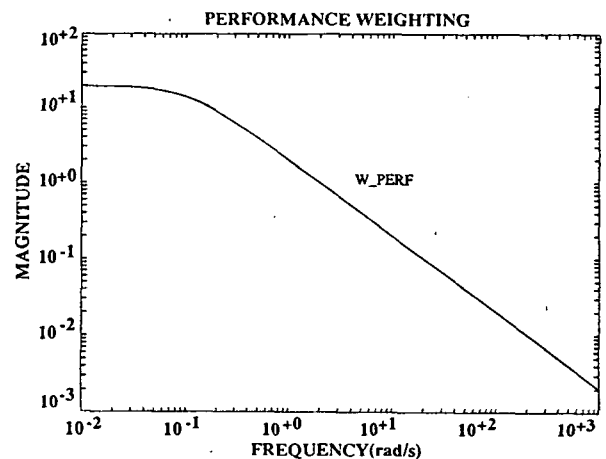


Figure 5. Performance weighting.

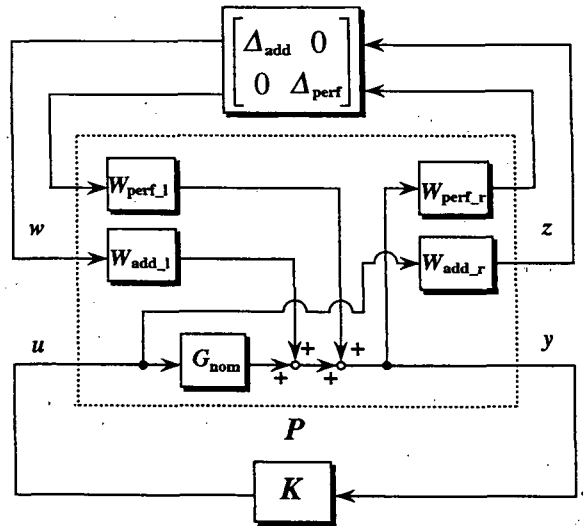


Figure 6. Interconnection structure.

Hence, the design objective is to find a controller  $K$  such that the closed-loop system remains internally stable for every  $G \in \mathbf{G}$ , and in addition the weighted sensitivity function satisfies the performance (11) for all  $G \in \mathbf{G}$ . This is the *robust performance* objective.

#### 4.2. BUILDING THE GENERALIZED PLANT

The above design goals exactly fit in the  $\mu$ -synthesis framework by introducing a fictitious uncertainty block  $\Delta_{perf}$ . The appended uncertainty block  $\Delta_{perf}$  is used to incorporate the robust performance calculation. Rearranging the feedback structure in Figure 4, we can build the interconnection structure shown in Figure 6. The open-loop interconnection  $P$  in Figure 6 is often referred to as the generalized plant.

### 5. DESIGN

#### 5.1. STRUCTURED SINGULAR VALUE ( $\mu$ )

First, define a block structure  $\underline{\Delta}$  as

$$\underline{\Delta} := \left\{ \begin{bmatrix} \Delta_{add} & 0 \\ 0 & \Delta_{perf} \end{bmatrix} : \Delta_{add} \in \mathbf{C}, \Delta_{perf} \in \mathbf{C} \right\}. \quad (12)$$

Next, with  $P$  partitioned as

$$P = \begin{bmatrix} P_{11} & P_{12} \\ P_{21} & P_{22} \end{bmatrix} \quad (13)$$

in an obvious way, let  $F_l(P, K)$  denote a linear fractional transformation on  $P$  by  $K$ , where

$$F_l(P, K) := P_{11} + P_{12}K(I - P_{22}K)^{-1}P_{21} \quad (14)$$

( see Figure 6 ). Then, robust performance is equivalent to the following structured singular value test [1]

$$\sup_{\omega \in \mathcal{R}} \mu_{\Delta} ( F_l ( P, K )( j\omega ) ) < 1. \quad (15)$$

Recall that, in this case, the structured singular value  $\mu_{\Delta}(M)$  is defined as

$$\mu_{\Delta}(M) := \frac{1}{\min \{ \bar{\sigma}(\Delta) : \Delta \in \underline{\Delta}, \det(I - M\Delta) = 0 \}} \quad (16)$$

for a matrix  $M \in \mathcal{C}^{2 \times 2}$ .

It is not known how to obtain a controller  $K$  achieving the structured singular value test (15) directly. Hence, our approach taken here is the so-called  $D$ - $K$  iteration [2]. Using the known upper bound for  $\mu$ , we can attempt to find a stabilizing controller  $K$  and a scaling matrix  $D$  such that

$$\| DF_l ( P, K ) D^{-1} \|_{\infty} \quad (17)$$

in minimized.

## 5.2. $\mu$ -ANALYSIS AND SYNTHESIS

The  $D$ - $K$  iteration involves a sequence of minimizations over either  $K$  or  $D$  while holding the other fixed, until a satisfactory controller is constructed. First, for  $D = I$  fixed, the controller  $K$  is synthesized using the well-known state-space  $H_{\infty}$  optimization method. Let  $F_l(P, K)$  be the closed-loop transfer function from the disturbances  $w$  to the errors  $z$  in Figure 6. Then, solving the following  $H_{\infty}$  control problem

$$\| F_l ( P, K ) \|_{\infty} < \gamma_1; \quad \gamma_1 = 1.3 \quad (18)$$

yields the central controller  $K_1$  below

$$K_1 = \frac{-7.31 \times 10^9 (s+84.4)(s+38.0)(s+35.0)(s+30.0)}{(s+1247.0)(s+23.8)(s+0.10)(s+603.7-j466.9)(s+603.7+j466.9)} \\ \times \frac{(s+18.0)(s+1.81)(s+0.697-j28.8)(s+0.697+j28.8)}{(s+42.7-j17.1)(s+42.7+j17.1)(s+0.397-j28.1)(s+0.397+j28.1)} \quad (19)$$

Thus, the first step of the  $D$ - $K$  iteration amounts to the standard  $H_{\infty}$  (sub)optimal control design. Now we try to assess robust performance of this closed-loop system using  $\mu$ -analysis associated with the block structure (12). The maximum singular value  $\bar{\sigma}$  and  $\mu$  of the closed-loop transfer function  $F_l(P, K_1)$  are plotted in Figure 7. It is noteworthy to point out that the peak value of the  $\mu$  plot is not less than 1! This reveals that the closed-loop system with  $K_1$  does not achieve robust performance [1], [2].

Next, the above calculations of  $\mu$  produce a scaling matrix at each frequency so as to minimize (17). These data will be fit with a stable, minimum-phase, real-rational function. The resulting scaling matrix  $D$  will be absorbed into the interconnection structure with multiplication and inverse. In this design, we try to fit the curve using a 1st order transfer function. Now, let  $P_2$  denote the new open-loop interconnection structure absorbing the scaling matrix  $D$ . This time, from the following  $H_{\infty}$  control problem

$$\|F_l(P_2, K)\|_\infty < \gamma_2; \quad \gamma_2 = 1.0 \quad (20)$$

we can calculate the central controller  $K_2$  as follows

$$K_2 = \frac{-6.93 \times 10^9 (s+84.4)(s+110.1)(s+2.85)(s+38.0)(s+35.0)(s+30.0)}{(s+1181.1)(s+24.6)(s+0.10)(s+110.5)(s+2.75)(s+578.6-j479.3)(s+578.6+j479.3)} \\ \times \frac{(s+18.0)(s+1.59)(s+0.697-j28.8)(s+0.697+j28.8)}{(s+41.3-j15.6)(s+41.3+j15.6)(s+0.421-j28.1)(s+0.421+j28.1)} \quad (21)$$

The maximum singular value  $\bar{\sigma}$  and  $\mu$  of this closed-loop transfer function are plotted in Figure 8. Further, in order to evaluate nominal performance as well as robust stability, the magnitudes of the frequency responses for the following four transfer functions are plotted in Figure 9 through 12

$$(I + G_{nom} K_i)^{-1} \quad (22)$$

$$(I + G_{nom} K_i)^{-1} G_{nom} \quad (23)$$

$$K_i (I + G_{nom} K_i)^{-1} \quad (24)$$

$$G_{nom} K_i (I + G_{nom} K_i)^{-1} \quad (25)$$

for  $i = 1, 2$ . From Figure 9 through 12, it can be seen that  $K_2$  achieves better nominal performance and robust stability than  $K_1$  does. Furthermore, since the value of  $\mu$  is less than 1 across frequency in Figure 8, robust performance is now achieved for the closed-loop system with the controller  $K_2$ .

## 6. EXPERIMENTAL RESULTS

The designed continuous-time controllers  $K_1$  and  $K_2$  are discretized via the Tustin transform at the sampling rate of  $61 \mu s$  and  $80 \mu s$ , respectively. We first evaluate nominal performance of these controllers with a output response for a step-type disturbance. The disturbance is added to the experimental system as an applied voltage in the electromagnet, which in fact amounts to about 20 % of the steady-state force. Figure 13 shows the response of  $y = x_1$ , when the controller  $K_2$  is implemented. While, Figure 14 shows the response with the controller  $K_1$  in the same situation. Comparing these results, we can see that  $K_2$  achieves better nominal performance.

Our concerns are also in the robustness of the closed-loop system against various real perturbations. Hence we further continue the same experiments with the values of the parameters in the experimental system changed. Based on this, we will evaluate robust performance as well as robust stability of the closed-loop system with the controller  $K_2$ . Noting the results in Section 3 regarding model perturbations, the parameters have been changed in the following ways:

- (i)  $m = 8.28$  kg, which amounts to 42.8 % increase for its nominal value of 5.80 kg,
- (ii)  $R = 59.5 \Omega$ , which amounts to 4.4 % increase for its nominal value of 57.0  $\Omega$ .

The experimental results are shown in Figure 15 and 16. In each case, it can be seen that the flexible beam is still suspended stably even though the step-type disturbance is added, and in addition to it, the transient behavior is not so deteriorated as compared with the result in Figure 13. Therefore, these experimental results confirm us that the closed-loop system with the controller  $K_2$  achieves robust performance.

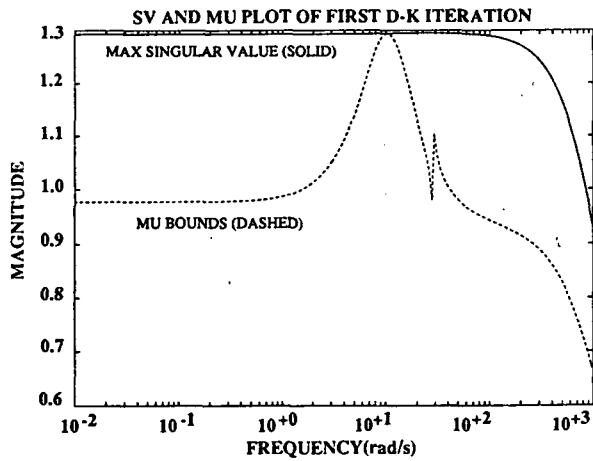


Figure 7.  $\bar{\sigma}$  and  $\mu$  plot of first *D-K* iteration.

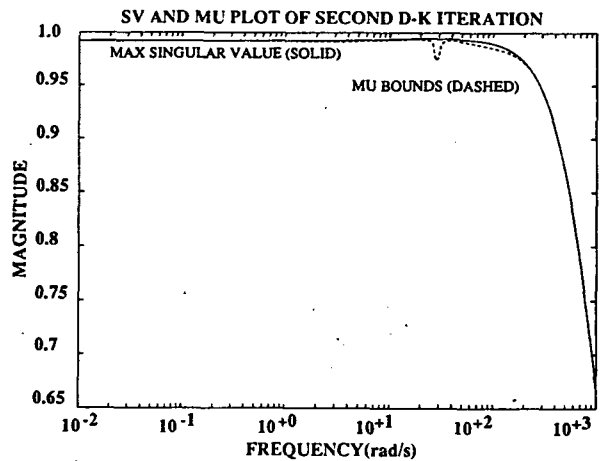


Figure 8.  $\bar{\sigma}$  and  $\mu$  plot of second *D-K* iteration.

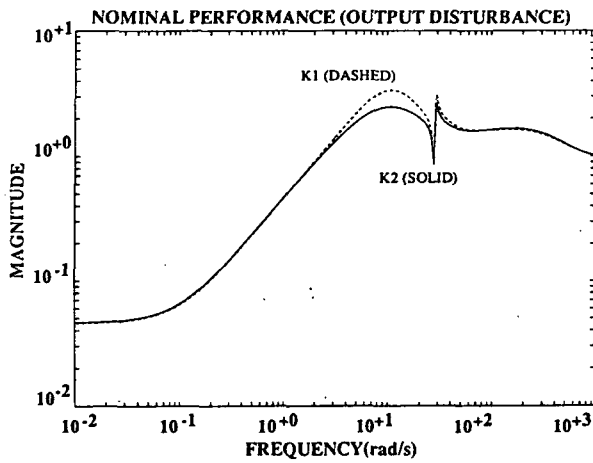


Figure 9.  $(I + G_{nom}K_i)^{-1}$  ( $i = 1, 2$ ).

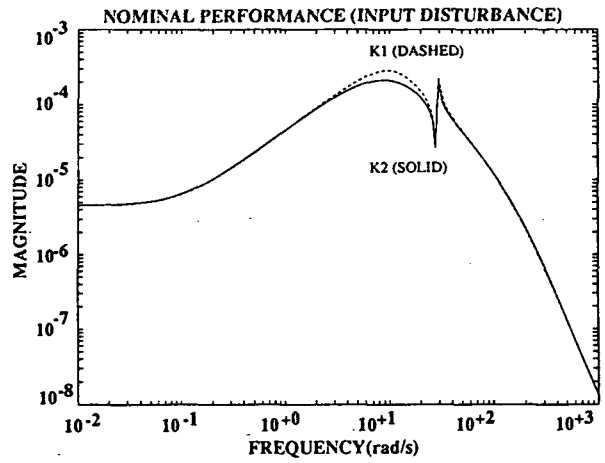


Figure 10.  $(I + G_{nom}K_i)^{-1}G_{nom}$  ( $i = 1, 2$ ).

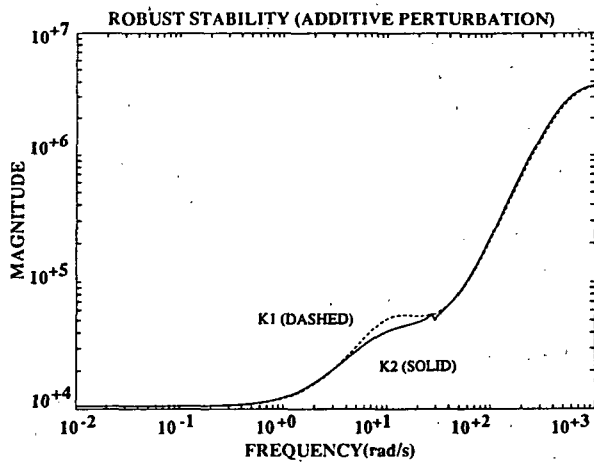


Figure 11.  $K_i(I + G_{nom}K_i)^{-1}$  ( $i = 1, 2$ ).

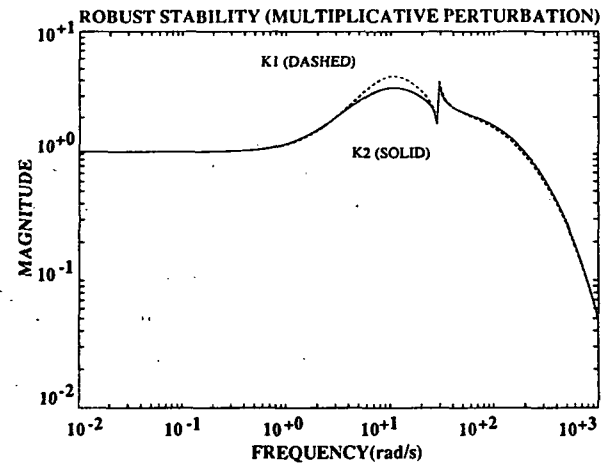


Figure 12.  $G_{nom}K_i(I + G_{nom}K_i)^{-1}$  ( $i = 1, 2$ ).

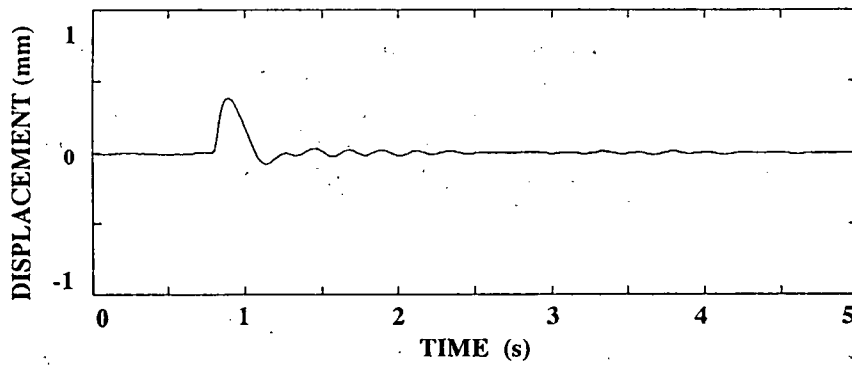


Figure 13. Output response to step disturbance with  $K_2$  ( nominal ).

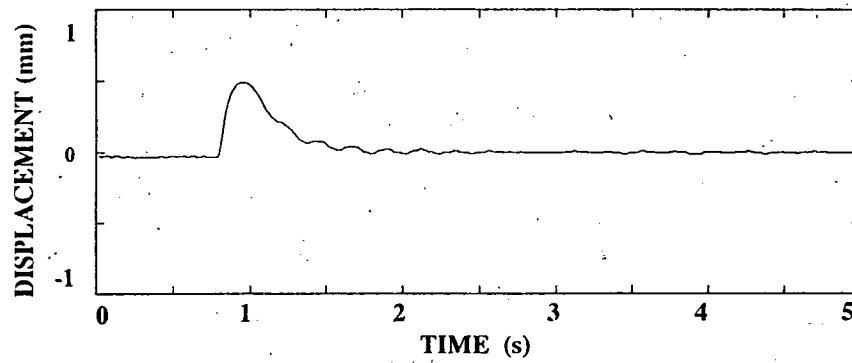


Figure 14. Output response to step disturbance with  $K_1$  ( nominal ).

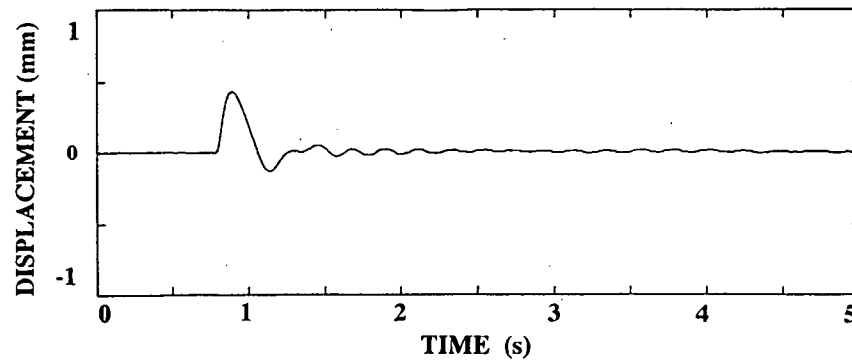


Figure 15. Output response to step disturbance with  $K_2$  ( perturbed:  $m = 8.28$  kg ).

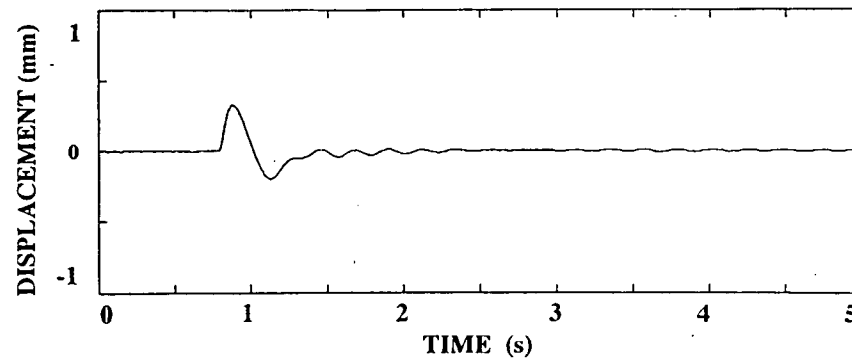


Figure 16. Output response to step disturbance with  $K_2$  ( perturbed:  $R = 59.5$  kg ).

## 7. CONCLUSIONS

In this paper, we evaluate a controller designed by  $\mu$ -synthesis methodology with experiments for a flexible beam magnetic suspension system. Several experimental results showed that the closed-loop system with the  $\mu$ -controller achieves not only nominal performance and robust stability, but in addition robust performance. For real practical applications of  $\mu$  to the magnetic suspension technology, we will need further experimental evaluation.

## REFERENCES

- [1] Doyle, J.C., A. Packard, and K. Zhou. December 1991. "Review of LFTs, LMIs, and  $\mu$ ," *Proc. 30th IEEE Conference on Decision and Control*, Brighton, England.
- [2] Balas, G.J., J.C. Doyle, K. Glover, A. Packard, and R. Smith. 1991.  *$\mu$ -Analysis and Synthesis Toolbox*, Minneapolis, MN: MUSYN Inc..
- [3] Fujita, M., F. Matsumura, and M. Shimizu. July 1990. " $H^\infty$  Robust Control Design for a Magnetic Suspension System," *Proc. 2nd International Symposium on Magnetic Bearings*, Tokyo, Japan.
- [4] Fujita, M., F. Matsumura, and K. Uchida. December 1990. "Experiments on the  $H^\infty$  Disturbance Attenuation Control of a Magnetic Suspension System," *Proc. 29th IEEE Conference on Decision and Control*, Honolulu, Hawaii.
- [5] Fujita, M., F. Matsumura, and K. Uchida. June 1991. "Experimental Evaluation of  $H^\infty$  Control for a Flexible Beam Magnetic Suspension System," *Proc. SICE Workshop on Robust Control*, Tokyo, Japan.